CHAPTER VII

Numerical Investigation of Heat and Mass Transfer of Three Dimensional MHD Free Convective Flow over a Flat Porous Plate Embedded in a Porous Medium

7.1. Introduction

Three-dimensional flows provide more physical insights of the real world problems when compared with two-dimensional flows. Three-dimensional flows have many applications in the field of aeronautical engineering, glass-fiber production, geophysics, science and technology. The study of heat and mass transfer in MHD flows has numerous applications in many industries such as geophysics, crude oil purifications, design of heat exchangers, pumps, power generators, flow meters, aeronautics, chemical engineering, etc., Detailed studies have been conducted in this area by many researchers due to its wide spread applications.

The steady two-dimensional laminar flow of an incompressible, viscous fluid past a stretching sheet was studied by Crane (1970). Later, Ariel (1994) considered the effect of magnetic field of a viscoelastic fluid past a stretching sheet with suction. Three-dimensional unsteady flow with heat and mass transfer over a continuous stretching surface was studied by Lakshmisha *et al*. (1988). Three-dimensional flow due to a stretching flat surface was studied by Wang (1984).

Three-dimensional flow of a viscous incompressible fluid through a porous medium bounded by two vertical walls, one wall being impermeable and the other is permeable was discussed by Guria *et al*. (2009). Chamkha (2000) studied the problem of transient, unsteady three-dimensional natural convection laminar fluid flow over an inclined permeable surface in the presence of MHD and resulting IVP was solved using implicit finite-difference method.

Unsteady three-dimensional MHD flow due to impulsive motion with heat and mass transfer in a saturated porous medium was studied by Rajagopal *et al.* (2013). MHD three-dimensional flow of heat transfer over a stretching surface in a viscoelastic fluid was studied by Ahmad and Nazar (2011). Steady three-dimensional flow for an incompressible, viscous fluid past a stretching sheet using the homotopy perturbation method was studied by Donald Ariel (2007).

The above mentioned studies have ignored the effect of magnetic field and porosity on three-dimensional steady flow. This gap motivates us to take up the present work wherein we study the effect of magnetic field on three-dimensional steady flow along with heat and mass transfer over a porous plate embedded in a porous medium. In order to examine the accuracy of our result, the effect of stretching ratio on velocities $f'(\eta), g'(\eta)$ are calculated and plotted. The results obtained are validated for vanishing magnetic field and porosity parameter which are found to be in good agreement with the results obtained by Donald Ariel (2007). In the present work, temperature and mass concentration are also taken into an account.

7.2. Flow Description and Governing Equations

We consider a steady three dimensional laminar flow of an incompressible viscous electrically conducting fluid induced by the stretching of the flat surface in two lateral directions in an otherwise quiescent fluid. At the same time, the wall temperature is raised from T_∞ to T_w $(T_w > T_\infty)$ and the concentration is raised from C_∞ to C_w $(C_w > C_\infty)$.The magnetic field is applied in the z-direction. We can neglect the effect of the induced magnetic field in comparison to the applied magnetic field. The electrical current flowing in the fluid gives rise to an induced magnetic field if the fluid were an electrical insulator, but here we have taken the fluid to be electrically conducting.

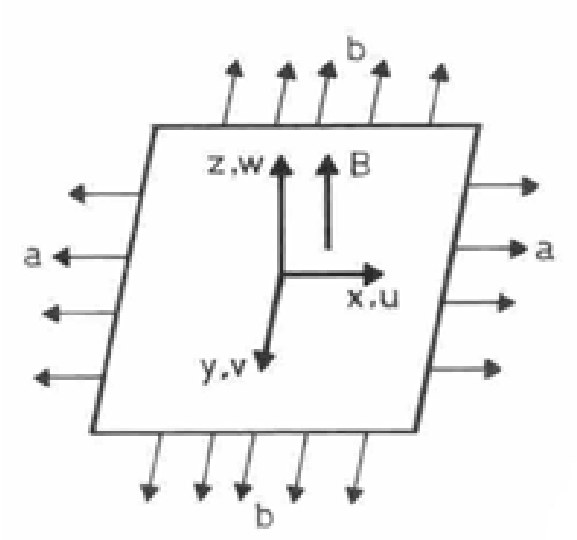

Fig 7.1 Physical Configuration of the problem

In the present work, the following assumptions are made:

- Flow of a Newtonian and electrically conducting fluid is considered which is three dimensional, steady, viscous, incompressible electrically conducting and laminar in nature.
- Fluid is induced by the stretching of the flat surface in two lateral directions in an otherwise quiescent fluid.
- The body forces are neglected.
- Heat source is assumed to be absent.
- Effect of Thermal diffusion are considered.
- Magnetic field is applied in the z-direction.
- The effect of the induced magnetic field is neglected in comparison to the applied magnetic field.
- The wall temperature is raised from T_∞ to T_w $(T_w > T_\infty)$
- The concentration is raised from C_∞ to C_w $(C_w > C_\infty)$.

Under these assumptions, the governing equations for the continuity, momentum and energy can be written as follows:

$$\frac{\partial u}{\partial x} + \frac{\partial v}{\partial y} + \frac{\partial w}{\partial z} = 0 \tag{7.1}$$

$$u\frac{\partial u}{\partial x} + v\frac{\partial u}{\partial y} + w\frac{\partial u}{\partial z} = \gamma\frac{\partial^2 u}{\partial z^2} - \frac{\sigma B_0^2}{\rho}u - \frac{\gamma}{k}u \tag{7.2}$$

$$u\frac{\partial v}{\partial x} + v\frac{\partial v}{\partial y} + w\frac{\partial v}{\partial z} = \gamma\frac{\partial^2 v}{\partial z^2} - \frac{\sigma B_0^2}{\rho}v - \frac{\gamma}{k}v \tag{7.3}$$

$$u\frac{\partial T}{\partial x} + v\frac{\partial T}{\partial y} + w\frac{\partial T}{\partial z} = \frac{\kappa}{\rho C_p}\frac{\partial^2 T}{\partial z^2} \tag{7.4}$$

$$u\frac{\partial C}{\partial x} + v\frac{\partial C}{\partial y} + w\frac{\partial C}{\partial z} = D_M\frac{\partial^2 C}{\partial z^2} + D_T\frac{\partial^2 T}{\partial z^2} \tag{7.5}$$

where T, C, μ, σ and $\gamma = (\mu/\rho)$ represent respectively the temperature, mass concentration, coefficient of viscosity, electrical conductivity and the kinematic viscosity of the fluid. The constant parameters in the system: $k, C_p, \kappa,$ D_M and D_T respectively denote the permeability of porous material, specific heat at constant pressure, thermal conductivity of the fluid, molecular diffusivity and thermal diffusivity.

The appropriate boundary conditions are given by,

$$u = u_w(x) = ax\,, \quad v = v_w(y) = by,\ T = T_w(x)\,, C = C_w(x) \text{ at } z = 0 \tag{7.6}$$

$$u \to 0,\ v \to 0,\ w \to 0, T \to T_\infty\,,\ C \to C_\infty \text{ as } z \to \infty\,, \tag{7.7}$$

7.3. Solution of the Problem

We use similarity technique to solve the system of equations (7.1)-(7.5) along with the boundary conditions (7.6) and (7.7). The similarity transformations are,

$$\eta = \sqrt{\frac{a}{\gamma}}\, z\ , u = axf'(\eta), v = byg'(\eta),$$

$$w = -\sqrt{a\gamma}\,[f(\eta) + cg(\eta)],\ \theta(\eta) = \frac{T-T_\infty}{T_w-T_\infty}, \phi(\eta) = \frac{C-C_\infty}{C_w-C_\infty} \qquad (7.8)$$

where $c = b/a$ is the stretching ratio of the velocities in y and x- directions, and prime denote differentiation with respect to η. Making use of (7.6) and (7.7), equation of continuity is identically satisfied and introducing the above transformations in equations (7.2)-(7.5) along with boundary conditions (7.6) and (7.7) we obtain the system of ordinary differential equations,

$$f''' + (f + cg)f'' - f'^2 - (M + k^*)f' = 0, \qquad (7.9)$$

$$g''' + (f + cg)g'' - cg'^2 - (M + k^*)g' = 0, \qquad (7.10)$$

$$\theta'' + Pr(f + cg)\theta' = 0, \qquad (7.11)$$

$$\phi'' + Sc(f + cg)\phi' + ScSr\theta'' = 0. \qquad (7.12)$$

The transformed boundary conditions are given as,

$$f(\eta) = 0,\ f'(\eta) = 1,\ g(\eta) = 0,\ g'(\eta) = c, \theta(\eta) = 1,\ \phi(\eta) = 1 \text{ at } \eta = 0; \qquad (7.13)$$

$$f'(\eta) \to 0,\ g'(\eta) \to 0, \theta(\eta) \to 0,\ \phi(\eta) \to 0 \quad \text{as } \eta \to \infty \qquad (7.14)$$

where $M = \frac{\sigma B_0^2}{a\rho}$ is the magnetic parameter, $Pr = \mu C_p/\kappa$ is the Prandtl number, $Sc = \frac{\gamma}{D_m}$ is the Schmidt number, $Sr = \frac{(T_w-T_\infty)D_T}{(C_w-C_\infty)\gamma}$ is the Soret number, $k^* = \gamma/ka$ is the permeability of porous medium and $Re_x = \frac{bx^2}{\gamma}$ is the Reynolds number.

The non-linear coupled ordinary differential equations (7.9)-(7.12) subject to boundary conditions (7.13)-(7.14) are reduced to a system of first order ordinary differential equations as follows,

$$f' = w,\ w' = v, g' = a,\ a' = A, \theta = y,\ \theta' = z,\ \phi = b,\ \phi' = e$$

$$v' = -(x + ci)v + w^2 + (M + k^*)w \qquad (7.15)$$

$$A' = -(x + ci)A + ca^2 + (M + k^*)a \qquad (7.16)$$

$$z' = -(Prx + Prci)z, \qquad (7.17)$$

$$e' = -(Scx + Scci)e + (ScSrPrx + ScSrPrci)z \qquad (7.18)$$

and boundary conditions become,

$$x(0) = 0,\ \ w(0) = 1, i(0) = 0, a(0) = 1, y(0) = 1,\ \ b(0) = 1 \ \text{ at } \eta = 0 \tag{7.19}$$

$$w(0) \to 0, a(0) \to 0, y(0) \to 0,\ \ b(0) \to 0 \quad \text{as } \eta \to \infty \tag{7.20}$$

We have solved the equations (7.15)-(7.18) with boundary conditions (7.19) and (7.20) using shooting method.

The major physical quantities - the skin-friction coefficient C_f, the local Nusselt number Nu_x, and the local Sherwood number Sh_x are defined respectively as follows,

Expressions for skin-friction coefficient C_f on the surface along x and y directions, which are denoted by C_{fx} and C_{fy} respectively are as follows:

$$C_{fx} = \frac{\tau_{wx}}{\rho u_w^2}, C_{fy} = \frac{\tau_{wy}}{\rho u_w^2}$$

where τ_{wx} and τ_{wy} are the shear stress along x and y directions respectively.

Local Nusselt number: $Nu_x = \frac{x q_w}{k(T_w - T_\infty)}$

Local Sherwood number: $Sh_x = \frac{x q_m}{D(C_w - C_\infty)}$

where q_w is the heat flux, q_m is the mass flux at the surface respectively.

$$\tau_{wx} = \mu \left(\frac{\partial u}{\partial z}\right)_{z=0}, \tau_{wy} = \mu \left(\frac{\partial v}{\partial z}\right)_{z=0}, \ q_w = -k \left(\frac{\partial T}{\partial z}\right)_{z=0}, q_m = -D \left(\frac{\partial C}{\partial z}\right)_{z=0}$$

Applying the non-dimensional transformations (7.8) we obtain,

$$f''(0) = C_{fx}(Re_x)^{1/2}$$

$$cg''(0) = \left(\frac{x}{y}\right) C_{fy}(Re_x)^{1/2}$$

$$-\theta'(0) = Nu_x(Re_x)^{-1/2}$$

$$-\phi'(0) = xSh_x(Re_x)^{-1/2}$$

where $Re_x = \frac{x u_x(x)}{\gamma}$ is the local Reynolds number based on the stretching velocity $u_x(x)$.

7.4. Results and Discussion

In order to get the physical insight of the problem we have studied the velocity profiles $f'(\eta), g'(\eta)$, temperature profile $\theta(\eta)$ and concentration profile $\phi(\eta)$ against various parameters such as magnetic field M, stretching ratio c, Schmidt number Sc, Soret number Sr and porosity parameter k^*. The effect of various flow parameters on

velocity field, skin-friction, Nusselt number and Sherwood number are calculated numerically and discussed with the help of graphs.

We have shown the effect of stretching ratio on velocities through figures (7.2) and (7.3) for vanishing magnetic field and porosity parameter. It can be seen from the figures that the increase in stretching ratio decreases the main velocity $f'(\eta)$ and increases the cross flow velocity $g'(\eta)$. These results are in agreement with Donald Ariel (2007).

Figures (7.4)-(7.7) represent the effect of magnetic parameter M on main and cross flow velocities $f'(\eta), g'(\eta)$, temperature and concentration profiles. It is observed that the increase in magnetic parameter M, causes decrease in velocity profiels $f'(\eta), g'(\eta)$, and increase in temperature $\theta(\eta)$ and concentration $\phi(\eta)$ profiles. It is evident that an increase in the magnetic parameter depreciates velocity and enhances the temperature and concentration profiles. We can observe that the enhancement of Lorentz force slows down the motion of electrically conducting fluids.

Figures (7.8)-(7.11) show the effect of stretching ratio parameter c on velocity profiles $f'(\eta), g'(\eta)$, temperature profile $\theta(\eta)$ and concentration profile $\phi(\eta)$. It is clear that an increase in stretching ratio decreases main velocity $f'(\eta)$, temperature $\theta(\eta)$ and concentration $\phi(\eta)$ profiles and increases cross flow velocity profile $g'(\eta)$.

Figures (7.12) and (7.13) exhibit the effect of Schmidt number Sc and Soret number Sr on concentration profiles. These two figures illustrate that the increase in Schmidt number Sc and Soret number Sr causes the decrease and increase in concentration profiles respectively.

Figures (7.14)-(7.17) exhibit the effect of porosity parameter k^* on velocity profiles $f'(\eta), g'(\eta)$, temperature profile $\theta(\eta)$ and concentration profile $\phi(\eta)$. It is evident that an increase in porosity parameter k^* decreases main flow and cross flow velocities $f'(\eta), g'(\eta)$ and reverse action can be observed in temperature $\theta(\eta)$ and concentration $\phi(\eta)$ profiles. However, the effect of porosity parameter on temperature and concentration distributions are not very significant.

Figures (7.18)-(7.21) depict the skin-friction $f''(0), g''(0)$, rate of heat transfer $\theta'(0)$, and rate of mass transfer $\phi'(0)$ against c for various values of M. We observe that the skin-friction $f''(0)$ and $g''(0)$ decrease, due to increase in stretching ratio parameter c and magnetic parameter M. Increasing stretching ratio, decreases the rate

of heat transfer and increases the rate of mass transfer. Increasing magnetic parameter increases the rate of heat and mass transfer.

7.5. Conclusion

The three-dimensional steady free-convective laminar flow of an incompressible viscous and electrically conducting fluid with heat and mass transfer over a porous flat plate in the presence of a uniform magnetic field embedded in porous medium has been investigated numerically. The non-linear boundary layer equations together with the boundary conditions are reduced to a system of non-linear ordinary differential equations by using similarity transformations. The system of non-linear ordinary differential equations is solved by shooting procedure using fourth order Runge-Kutta Method. The results are obtained for the velocity, temperature and concentration profiles, the skin-friction coefficient, Nusselt number and the Sherwood number. Effect of various non-dimensional parameters on the fluid flow, heat and mass transfer characteristics are examined.

The following conclusions are drawn from the present study:

- Main flow and cross flow velocities decrease when magnetic field increases, whereas temperature and concentration increase, with increasing magnetic field.
- The skin-friction $f''(0)$ and $g''(0)$ decrease with an increase in stretching ratio parameter and magnetic parameter.
- Increase in magnetic field and stretching ratio causes an increase in the rate of heat and mass transfer.

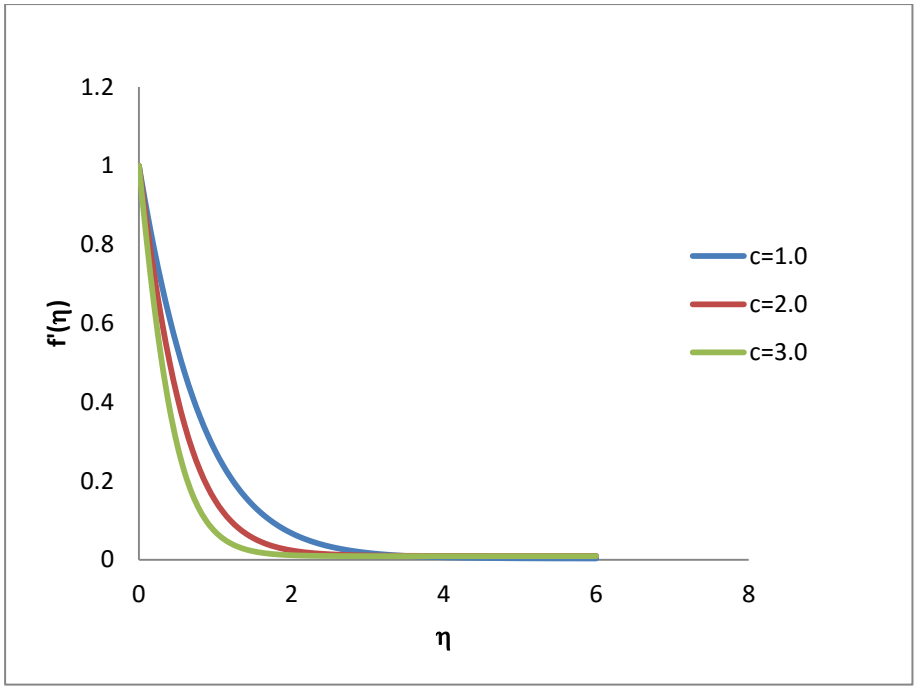

Fig 7.2 Effect of stretching ratio on velocity $f'(\eta)$. When M = k= 0*

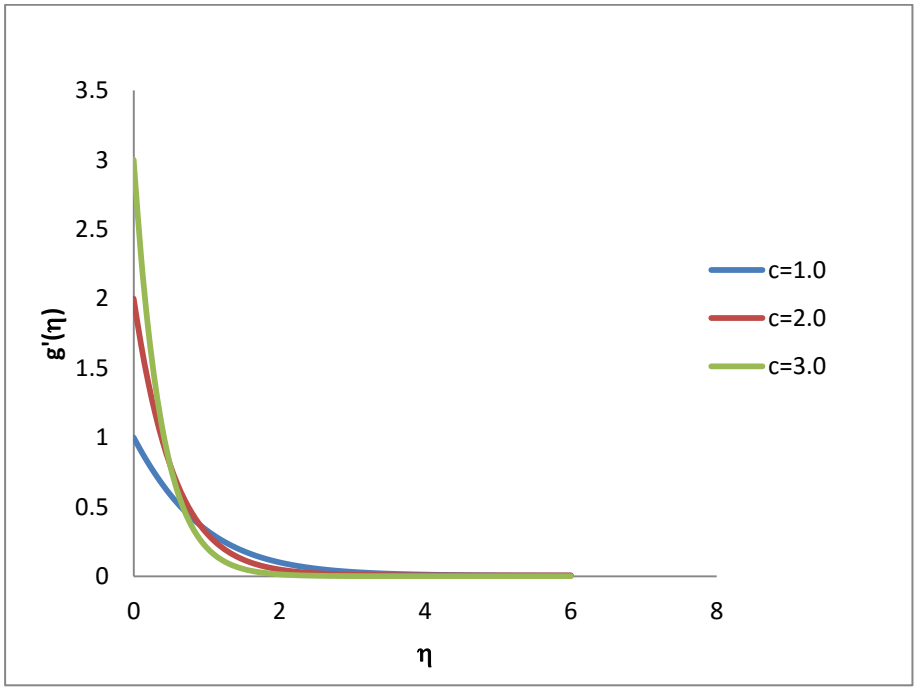

Fig 7.3 Effect of stretching ratio on velocity $g'(\eta)$. When M = k = 0*

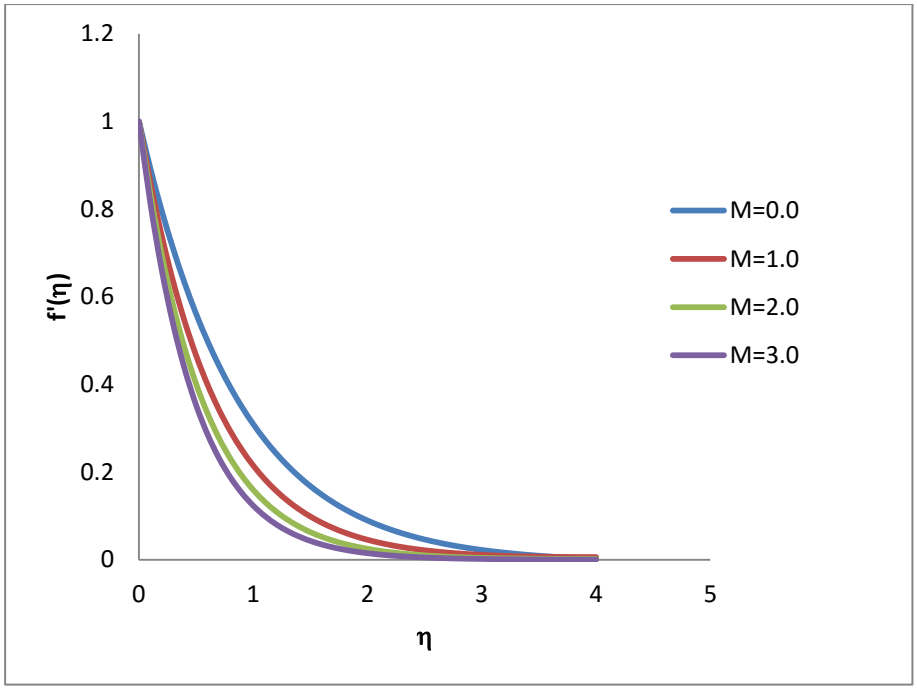

Fig 7.4 Effect of magnetic field on velocity $f'(\eta)$; Pr=7.0; k=0.2; Sc=0.3; Sr=0.3; c= 0.5*

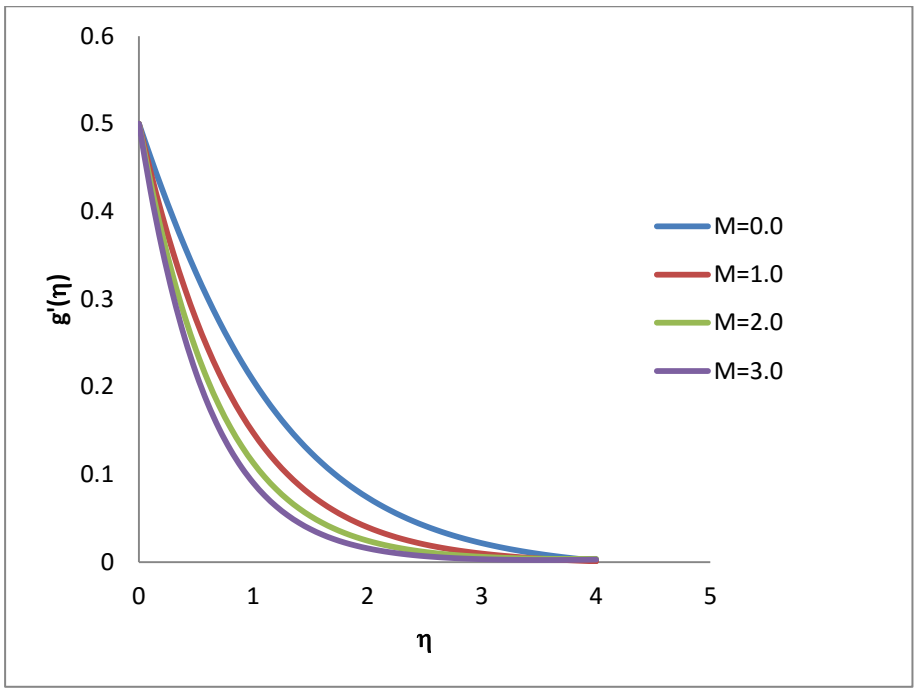

Fig 7.5 Effect of magnetic field on velocity $g'(\eta)$; Pr=7.0; k=0.2; Sc=0.3; Sr=0.3; c= 0.5*

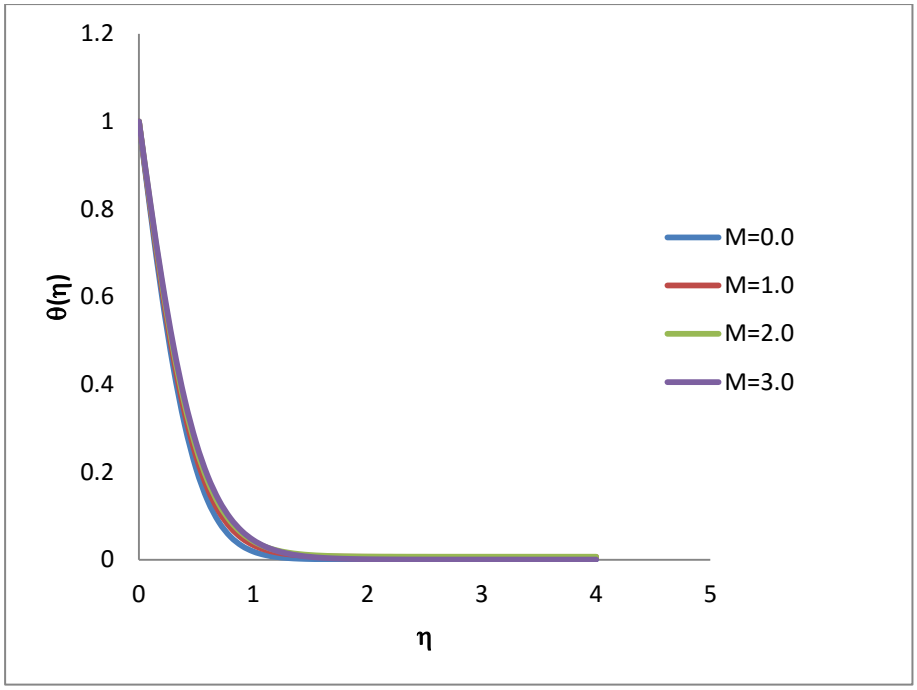

Fig 7.6 Effect of magnetic field on temperature $\theta(\eta)$; Pr=7.0; k=0.2; Sc=0.3; Sr=0.3; c= 0.5*

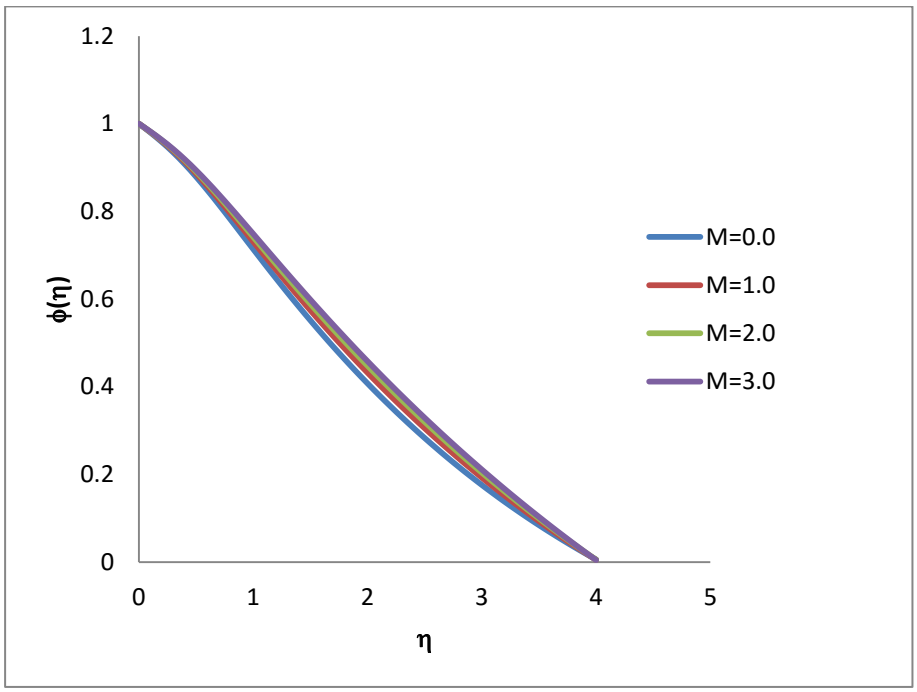

Fig 7.7 Effect of magnetic field on concentration $\phi(\eta)$; Pr=7.0; k=0.2; Sc=0.3; Sr=0.3; c= 0.5*

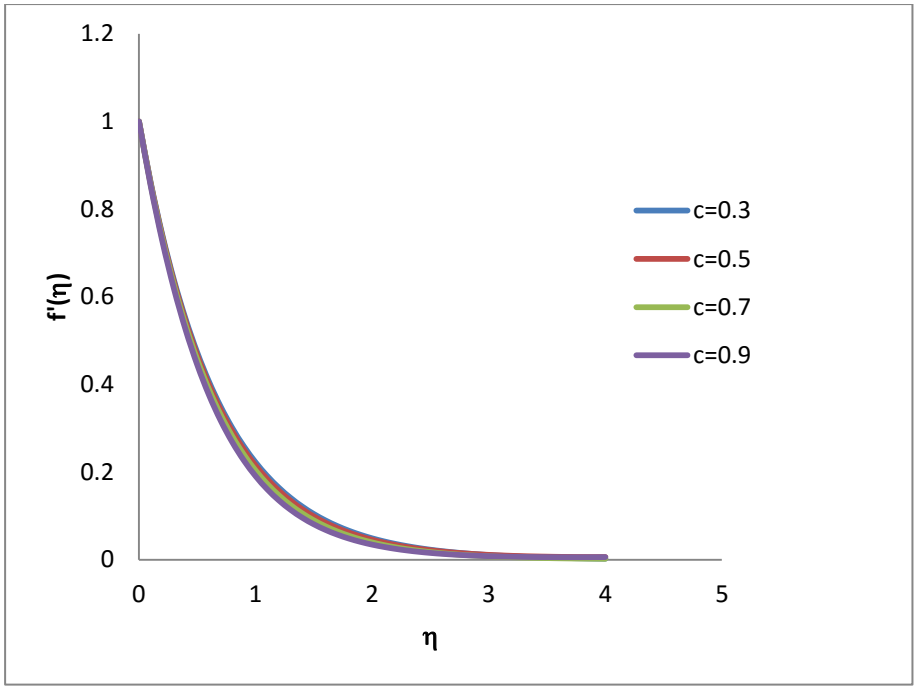

Fig 7.8 Effect of stretching ratio on velocity $f'(\eta)$; Pr=7.0; k=0.2; Sc=0.3; Sr=0.3; M= 1.0*

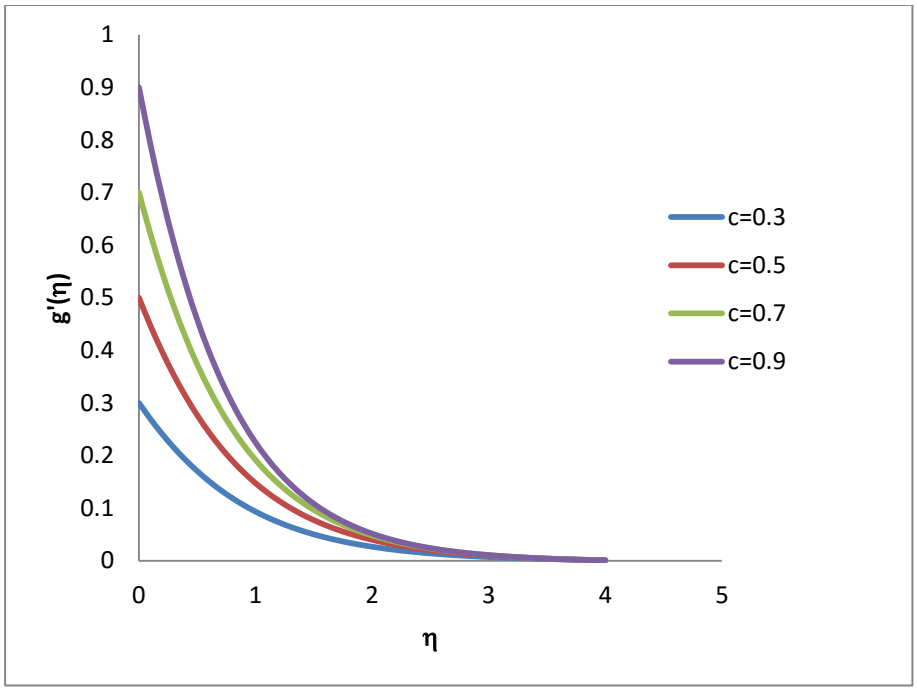

Fig 7.9 Effect of stretching ratio on velocity $g'(\eta)$; Pr=7.0; k=0.2; Sc=0.3; Sr=0.3; M= 1.0*

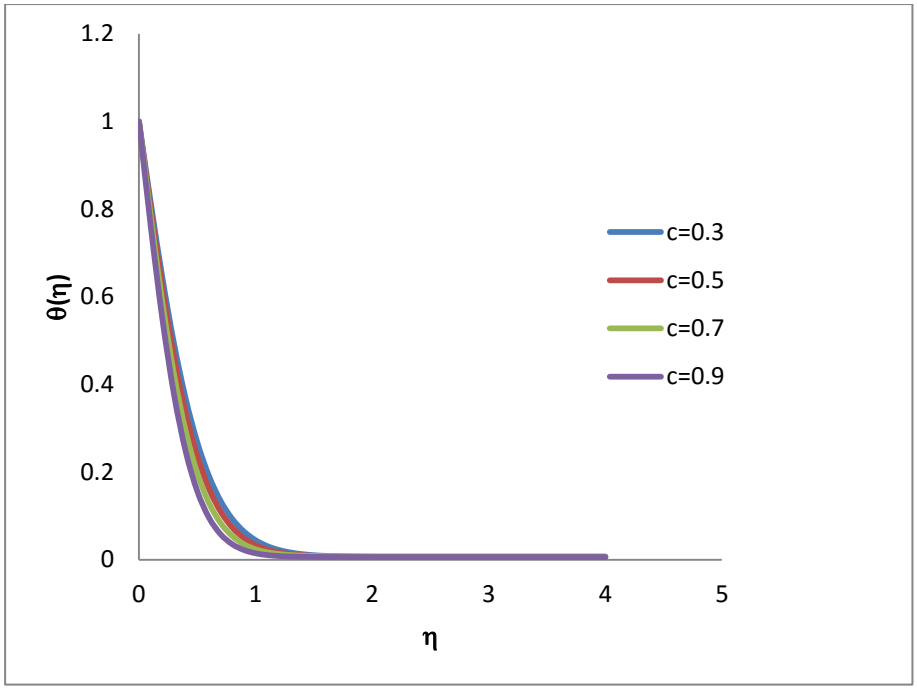

Fig 7.10 Effect of stretching ratio on temperature $\theta(\eta)$; Pr=7.0; k=0.2; Sc=0.3; Sr=0.3; M= 1.0*

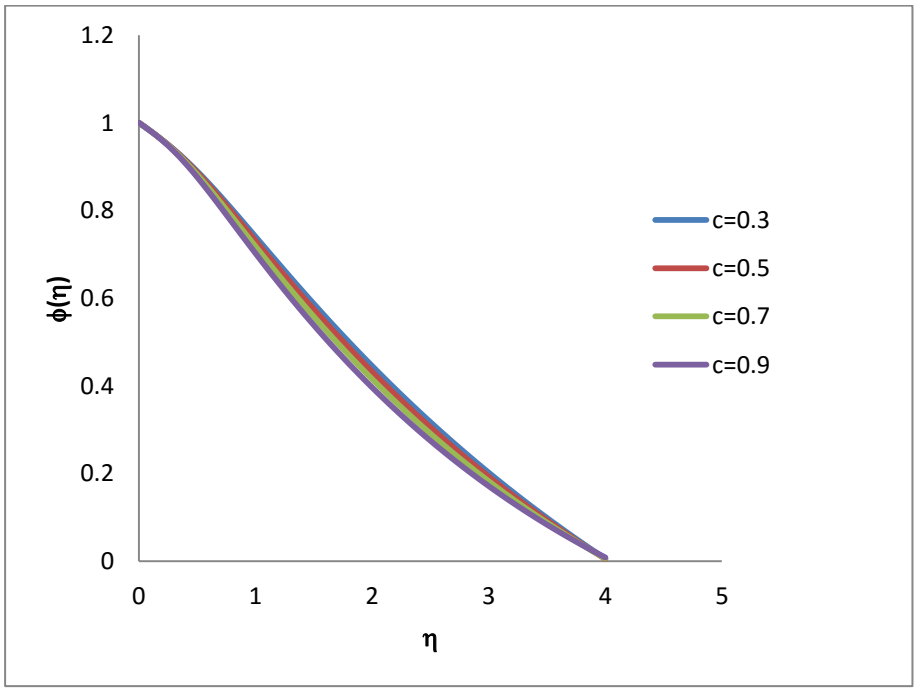

Fig 7.11 Effect of stretching ratio on concentration $\phi(\eta)$; Pr=7.0; k=0.2; Sc=0.3; Sr=0.3; M= 1.0*

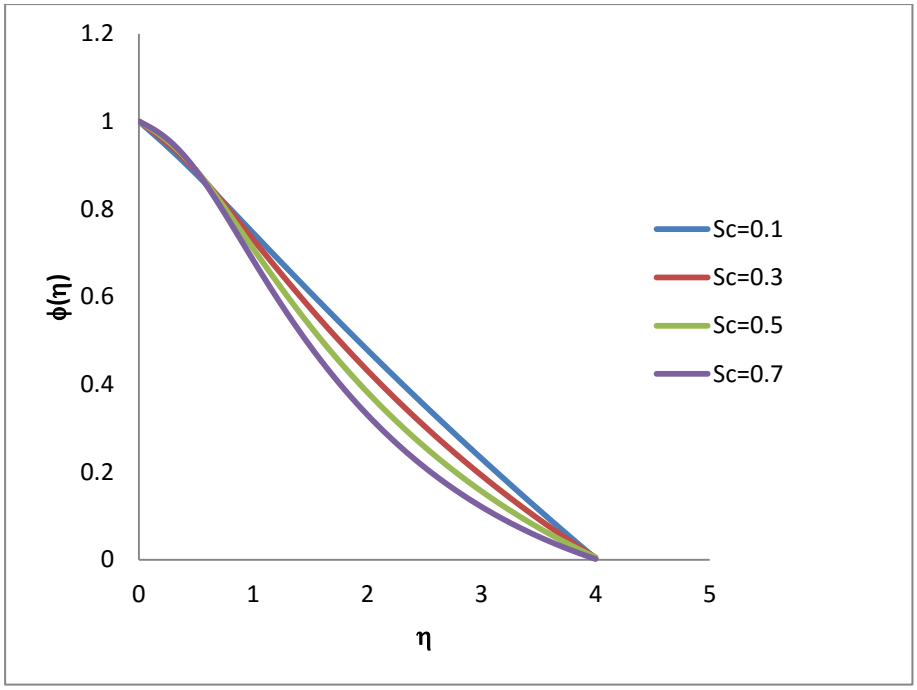

Fig 7.12 Effect of Schmidt number on concentration $\phi(\eta)$; Pr=7.0; k=0.2; c=0.5; Sr=0.3; M= 1.0*

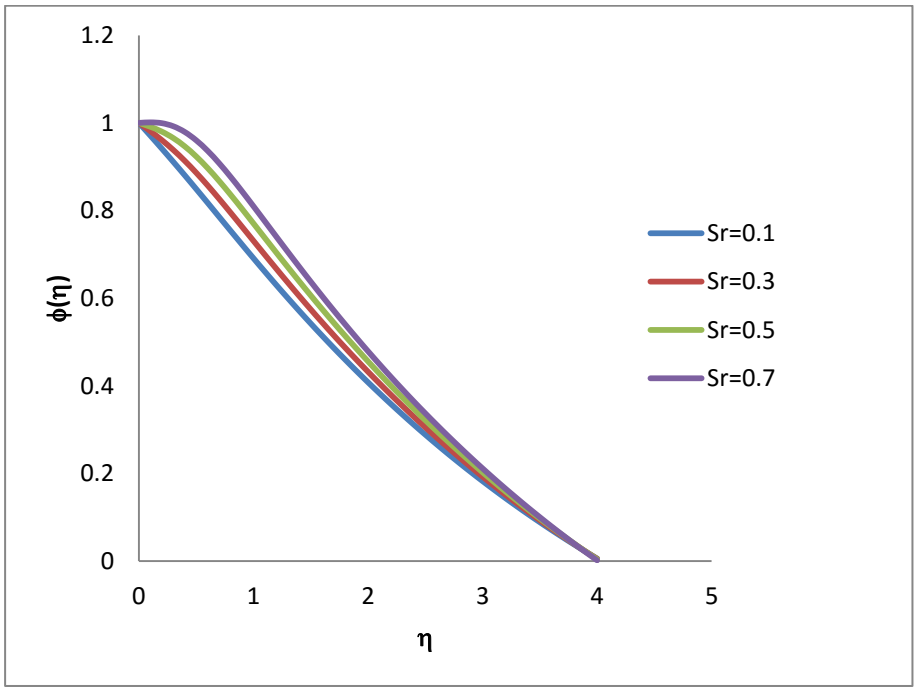

Fig 7.13 Effect of Soret number on concentration $\phi(\eta)$; Pr=7.0; k=0.2; c=0.5; Sc=0.3; M= 1.0*

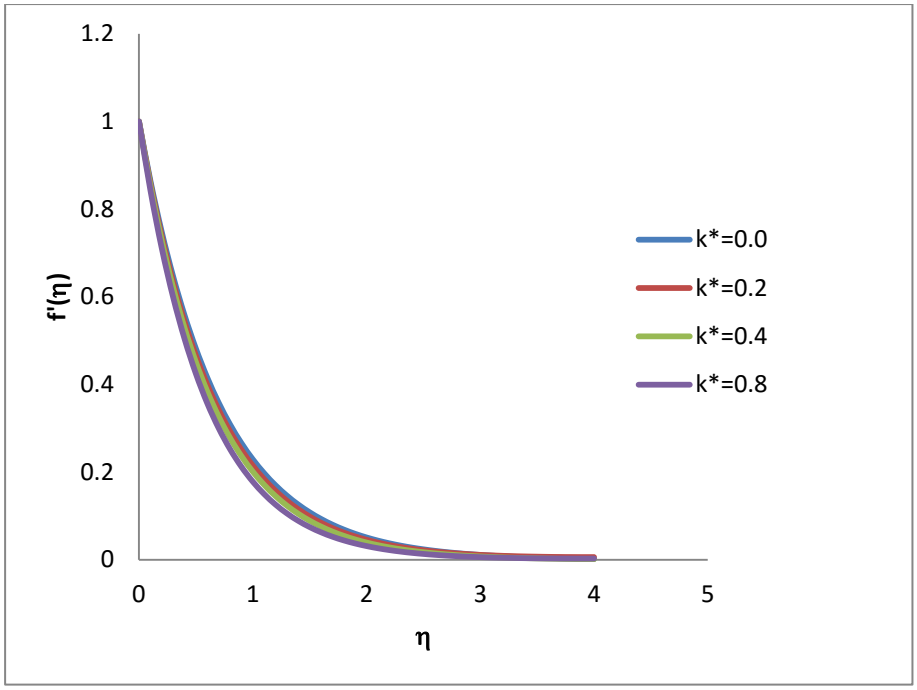

Fig 7.14 Effect of Porosity on velocity $f'(\eta)$; Pr=7.0; c=0.5; Sc=0.3; Sr=0.3; M= 1.0

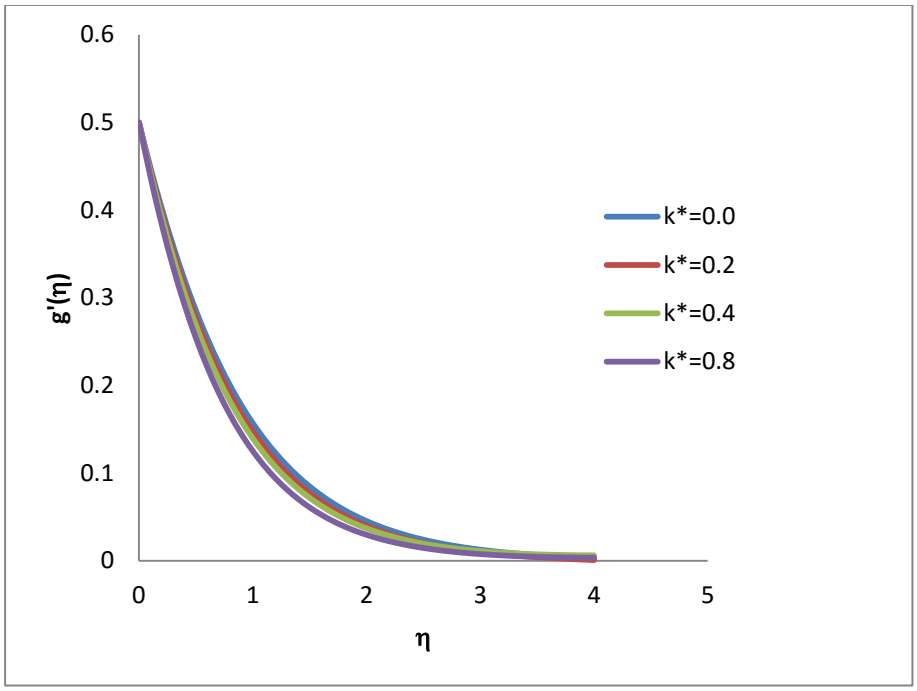

Fig 7.15 Effect of Porosity on velocity $g'(\eta)$; Pr=7.0; c=0.5; Sc=0.3; Sr=0.3; M= 1.0

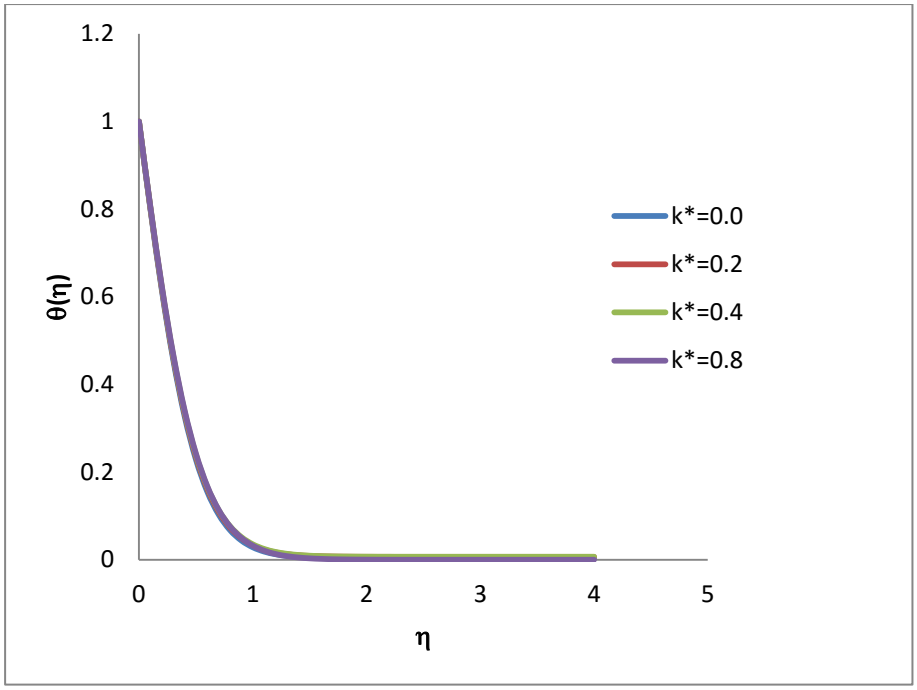

Fig 7.16 Effect of Porosity on temperature $\theta(\eta)$; Pr=7.0; c=0.5; Sc=0.3; Sr=0.3; M= 1.0

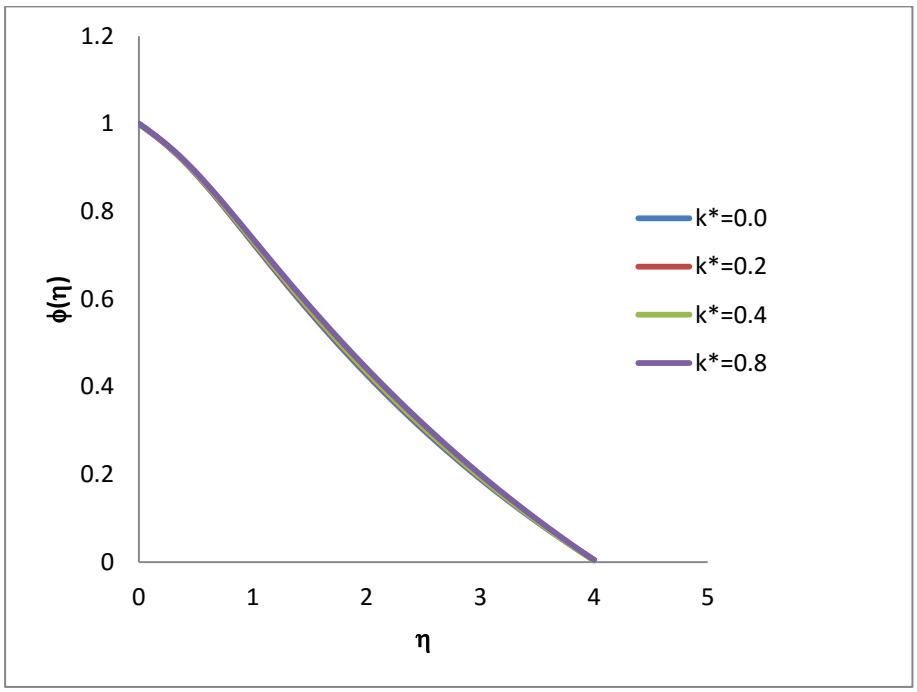

Fig 7.17 Effect of Porosity on concentration $\phi(\eta)$; Pr=7.0; c=0.5; Sc=0.3; Sr=0.3; M= 1.0

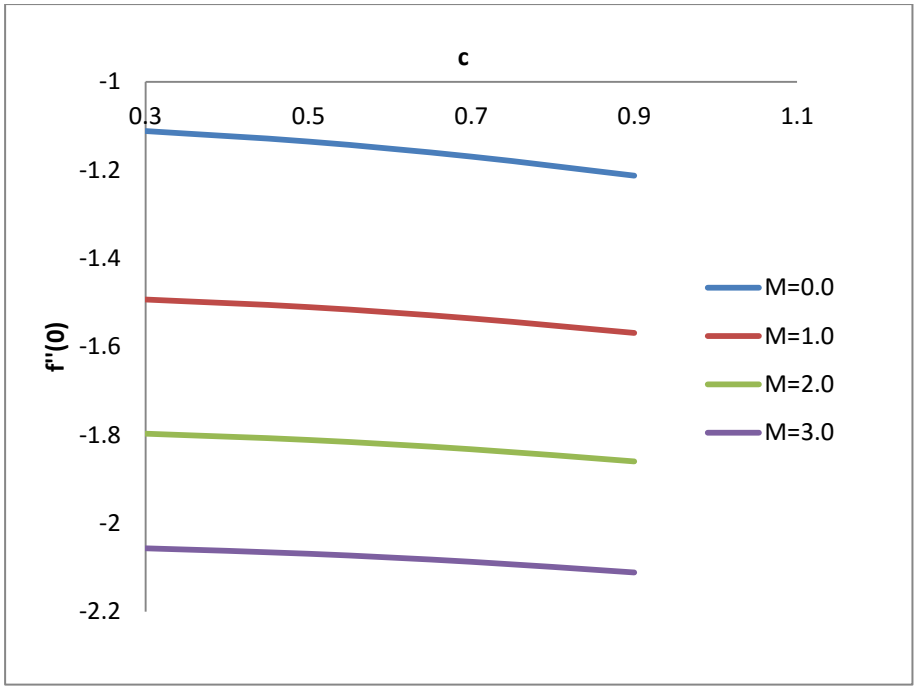

Fig 7.18 Skin-friction coefficient $f''(0)$ against c for various values of magnetic parameter M; Pr=7.0; Sc=0.3; Sr=0.3; k= 0.2*

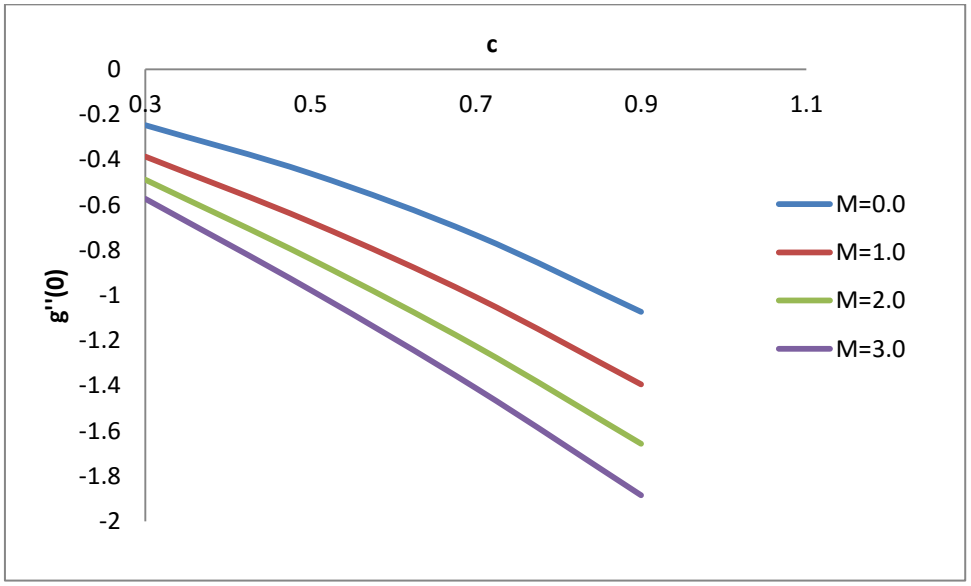

Fig 7.19 Skin-friction coefficient $g''(0)$ against c for various values of magnetic parameter M; Pr=7.0; Sc=0.3; Sr=0.3; k= 0.2*

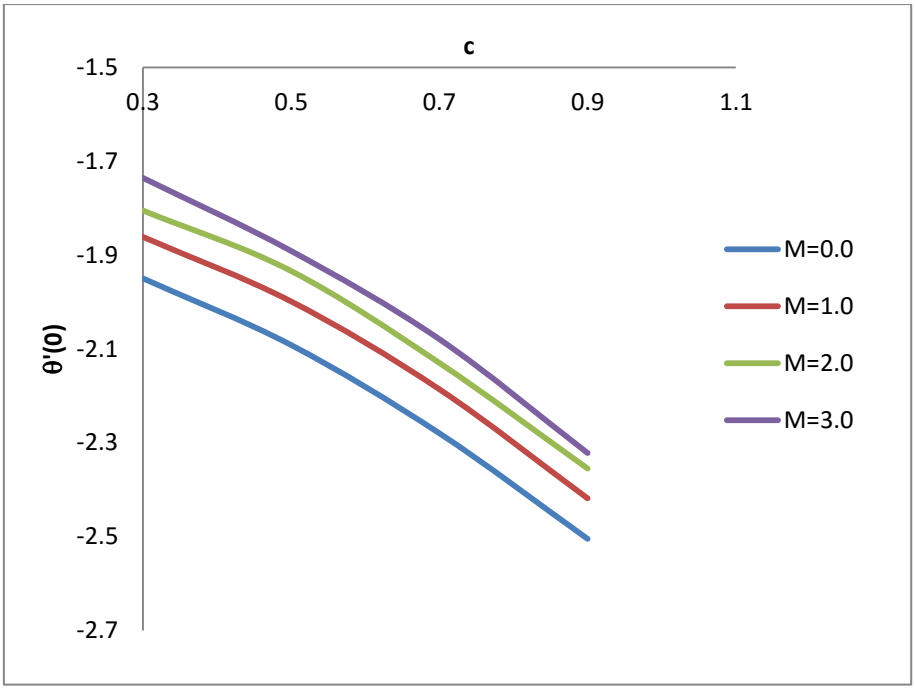

Fig 7.20 Rate of heat transfer $\theta'(0)$ against c for various values of magnetic parameter M; Pr=7.0; Sc=0.3; Sr=0.3; k= 0.2*

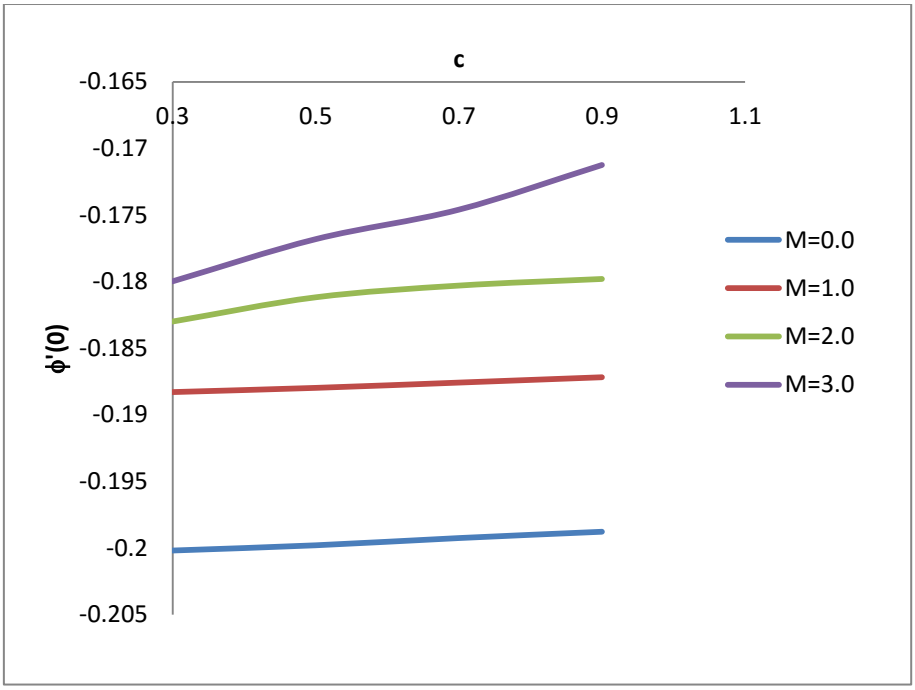

Fig 7.21 Rate of mass transfer $\phi'(0)$ against c for various values of magnetic parameterM; Pr=7.0; Sc=0.3; Sr=0.3; k= 0.2*